11-11-2022

Imprinted antibody responses against SARS-CoV-2 Omicron sublineages

Young-Jun Park
University of Washington
Zhuoming Liu
Washington University School of Medicine in St. Louis
Javier Janer
Washington University School of Medicine in St. Louis
Sean P J Whelan
Washington University School of Medicine in St. Louis
Herbert W Virgin
Washington University School of Medicine in St. Louis

See next page for additional authors

RESEARCH ARTICLE

CORONAVIRUS

Imprinted antibody responses against SARS-CoV-2 Omicron sublineages

Young-Jun Park[1,2]†, Dora Pinto[3]†, Alexandra C. Walls[1,2]†, Zhuoming Liu[4]†, Anna De Marco[3], Fabio Benigni[3], Fabrizia Zatta[3], Chiara Silacci-Fregni[3], Jessica Bassi[3], Kaitlin R. Sprouse[1], Amin Addetia[1], John E. Bowen[1], Cameron Stewart[1], Martina Giurdanella[3], Christian Saliba[3], Barbara Guarino[3], Michael A. Schmid[3], Nicholas M. Franko[5], Jennifer K. Logue[5], Ha V. Dang[6], Kevin Hauser[6], Julia di Iulio[6], William Rivera[6], Gretja Schnell[6], Anushka Rajesh[6], Jiayi Zhou[6], Nisar Farhat[6], Hannah Kaiser[6], Martin Montiel-Ruiz[6], Julia Noack[6], Florian A. Lempp[6], Javier Janer[4], Rana Abdelnabi[7], Piet Maes[7], Paolo Ferrari[9,10,11], Alessandro Ceschi[9,12,13,14], Olivier Giannini[9,15], Guilherme Dias de Melo[16], Lauriane Kergoat[16], Hervé Bourhy[16], Johan Neyts[7], Leah Soriaga[6], Lisa A. Purcell[6], Gyorgy Snell[6], Sean P.J. Whelan[4], Antonio Lanzavecchia[3], Herbert W. Virgin[6,17,18], Luca Piccoli[3], Helen Y. Chu[5], Matteo Samuele Pizzuto[3], Davide Corti[3]*, David Veesler[1,2]*

Severe acute respiratory syndrome coronavirus 2 (SARS-CoV-2) Omicron sublineages carry distinct spike mutations resulting in escape from antibodies induced by previous infection or vaccination. We show that hybrid immunity or vaccine boosters elicit plasma-neutralizing antibodies against Omicron BA.1, BA.2, BA.2.12.1, and BA.4/5, and that breakthrough infections, but not vaccination alone, induce neutralizing antibodies in the nasal mucosa. Consistent with immunological imprinting, most antibodies derived from memory B cells or plasma cells of Omicron breakthrough cases cross-react with the Wuhan-Hu-1, BA.1, BA.2, and BA.4/5 receptor-binding domains, whereas Omicron primary infections elicit B cells of narrow specificity up to 6 months after infection. Although most clinical antibodies have reduced neutralization of Omicron, we identified an ultrapotent pan-variant–neutralizing antibody that is a strong candidate for clinical development.

The emergence of the severe acute respiratory syndrome coronavirus 2 (SARS-CoV-2) Omicron variant at the end of 2021 caused a worldwide surge in COVID-19 cases. The Omicron BA.1 and BA.1.1 lineages swept the world first, followed by the BA.2 lineage (*1*). Although BA.1 and BA.2 share a large number of spike (S) mutations, they are each characterized by unique sets of amino acid changes that are associated with different antigenic properties (*2*–*4*). The BA.2.12.1 sublineage emerged in the United States, peaking at the beginning of June 2022, and is characterized by the presence of the L452Q receptor-binding domain (RBD) and S704L fusion machinery mutations in addition to the BA.2-defining mutations (*4*). The BA.2.75 sublineage is spreading in multiple countries and carries unique mutations (added to the BA.2 background) in the N-terminal domain (NTD), along with D339H, G446S, and N460K mutations and an R493Q reversion in the RBD (*5*). The BA.3 S glycoprotein comprises a combination of mutations found in BA.1 S and BA.2 S (*6*), whereas BA.4 S and BA.5 S are identical to each other and comprise a deletion of residues 69 to 70, L452R and F486V substitutions, and an R493Q reversion compared with BA.2 S (*7*). We characterized the emergence of Omicron (BA.1) as a major antigenic shift because of the unprecedented magnitude of immune evasion associated with this variant of concern (*3*, *8*–*12*). Mutations in the BA.1 S glycoprotein NTD and RBD, which are the main targets of neutralizing antibodies (*3*, *8*, *13*–*18*), explain the markedly reduced plasma-neutralizing activity of previously infected or vaccinated subjects (especially those who have not received booster doses) and the escape from most monoclonal antibodies (mAbs) used in the clinic. As a result, an increasing number of reinfections or breakthrough infections are occurring (*19*–*22*), even though these cases tend to be milder than infections of immunologically naive individuals.

Characterization of plasma and mucosal humoral responses to Omicron infection

Understanding the relationships between prior antigen exposure through vaccination or infection with one SARS-CoV-2 strain and the immune response to subsequent infections with a different strain is paramount to guiding strategies to end the COVID-19 pandemic. To investigate this, we first evaluated the magnitude of immune evasion associated with the Omicron sublineages by assessing the neutralizing activity of human plasma using a nonreplicative vesicular stomatitis virus (VSV) pseudotyped with Wuhan-Hu-1 S harboring G614 (Wu-G614), Delta, BA.1, BA.2, BA.2.12.1, or BA.4/5 mutations or with SARS-CoV S (Fig. 1A; fig. S1, A to G; table S1; and data S1). We compared plasma from six cohorts of individuals: those previously infected in 2020 (with a Washington-1–like SARS-CoV-2 strain) and then vaccinated twice ("infected-vaccinated 2 doses") or three times ("infected-vaccinated 3 doses); those who were vaccinated and then experienced either a Delta or an Omicron BA.1 breakthrough infection ("Delta breakthrough 3 doses," "BA.1 breakthrough 2 doses," and "BA.1 breakthrough 3 doses"); and those who had only been vaccinated and boosted ("vaccinated-only 3 doses"). Neutralizing antibody responses were slightly more robust against BA.2 S VSV than against BA.1 S VSV among all groups except for the BA.1 breakthrough cases. Reductions of geometric mean titers (GMTs) relative to Wu-G614 S VSV ranged from 1.4- to 8.2-fold against BA.1 and from 1.6- to 4-fold against BA.2 (Fig. 1A; fig. S1, A to G; table S1; and data S1), which is consistent with recent findings (*4*). BA.2.12.1 S VSV was associated with further reductions of plasma-neutralizing activity relative to BA.2 S VSV, whereas BA.4/5 S VSV had the greatest impact of all of the SARS-CoV-2 variants evaluated here, with GMT reductions of 5- to 14-fold relative to Wu-G614 S VSV (Fig. 1A; fig. S1, A to G; table S1; and data S1). All six cohorts experienced reductions in plasma-neutralizing GMT of 1.4- to 3.6-fold against Delta (*23*–*25*) relative to Wu-G614 S VSV, underscoring that even hybrid immunity [i.e., that acquired through vaccination and infection (*26*)] does not overcome evasion from neutralizing antibody responses of this previously dominant variant of concern (Fig. 1A; fig. S1, A to G; table S1; and data S1). The highest levels of neutralizing GMTs against SARS-CoV-2 variants were observed for BA.1 breakthrough cases, which was possibly due

[1]Department of Biochemistry, University of Washington, Seattle, WA, USA. [2]Howard Hughes Medical Institute, University of Washington, Seattle, WA, USA. [3]Humabs Biomed SA, Subsidiary of Vir Biotechnology, Bellinzona, Switzerland. [4]Department of Molecular Microbiology, Washington University School of Medicine, St. Louis, MO, USA. [5]Division of Allergy and Infectious Diseases, University of Washington, Seattle, WA, USA. [6]Vir Biotechnology, San Francisco, CA, USA. [7]KU Leuven Department of Microbiology, Immunology and Transplantation, Rega Institute for Medical Research, Laboratory of Virology and Chemotherapy, B-3000 Leuven, Belgium. [8]Laboratory of Clinical and Epidemiological Virology, Rega Institute, Department of Microbiology, Immunology and Transplantation, KU Leuven, Leuven, Belgium. [9]Faculty of Biomedical Sciences, Università della Svizzera italiana, Lugano, Switzerland. [10]Division of Nephrology, Ente Ospedaliero Cantonale, Lugano, Switzerland. [11]Clinical School, University of New South Wales, Sydney, New South Wales, Australia. [12]Clinical Trial Unit, Ente Ospedaliero Cantonale, Lugano, Switzerland. [13]Division of Clinical Pharmacology and Toxicology, Institute of Pharmacological Sciences of Southern Switzerland, Ente Ospedaliero Cantonale, Lugano, Switzerland. [14]Department of Clinical Pharmacology and Toxicology, University Hospital Zurich, Zurich, Switzerland. [15]Department of Medicine, Ente Ospedaliero Cantonale, Bellinzona, Switzerland. [16]Institut Pasteur, Université Paris Cité, Lyssavirus Epidemiology and Neuropathology Unit, F-75015 Paris, France. [17]Department of Pathology and Immunology, Washington University School of Medicine, St. Louis, MO, USA. [18]Department of Internal Medicine, UT Southwestern Medical Center, Dallas, TX, USA.
***Corresponding author. Email: dveesler@uw.edu (D.V.); dcorti@vir.bio (D.C.)**
†These authors contributed equally to this work.

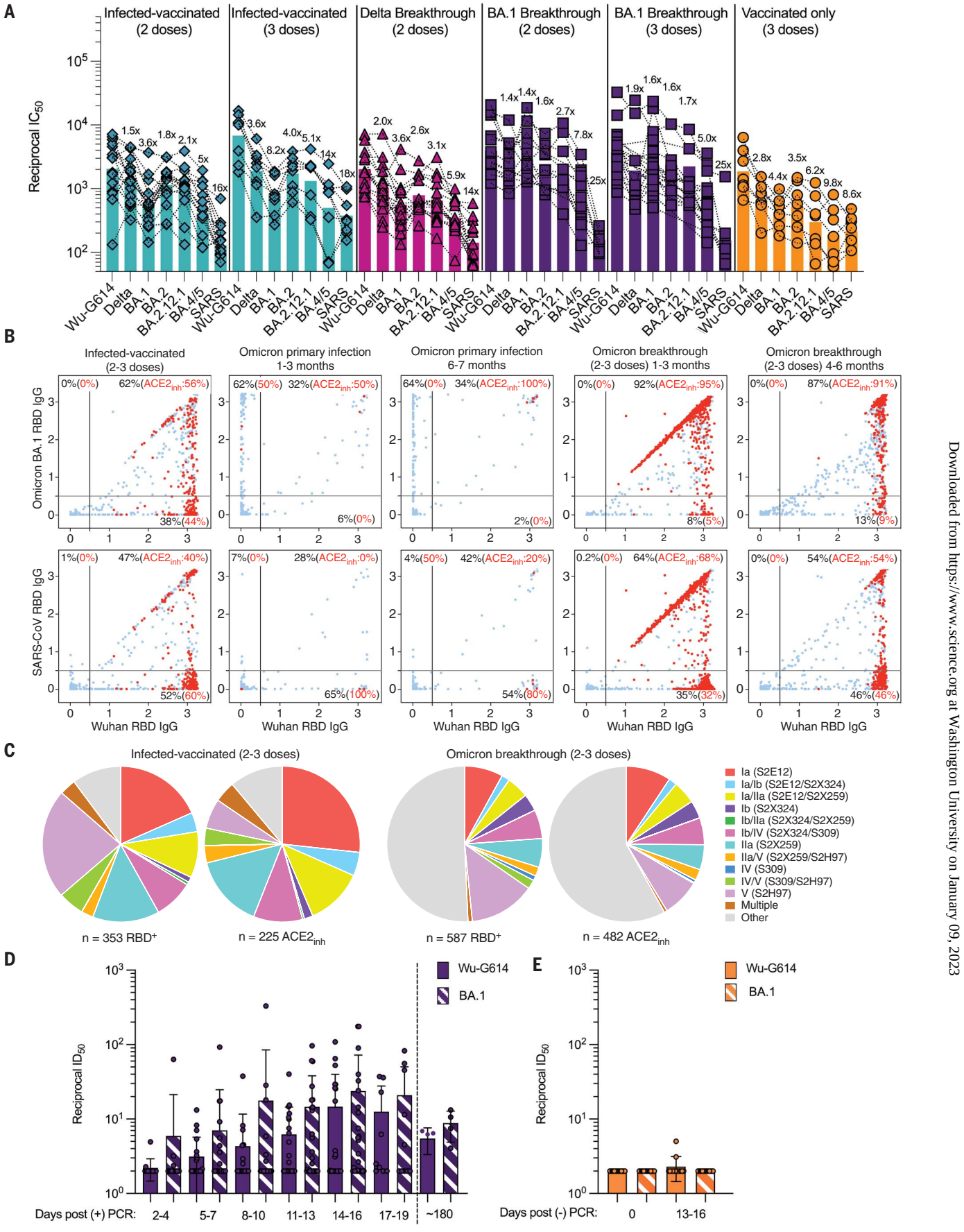

Fig. 1. Evaluation of plasma, memory, and mucosal antibody responses upon Omicron breakthrough infections in humans. (**A**) Pairwise neutralizing activity [half-maximum inhibitory dilution (ID_{50})] against Wu-G614, Delta, BA.1, BA.2, BA.2.12.1, BA.4/5, and SARS-CoV S VSV pseudoviruses using plasma from subjects who were infected and vaccinated, vaccinated and experienced breakthrough infection, or received vaccination only. VeroE6-TMPRSS2 cells were used as target cells (*93*). Data are the geometric mean of an $n = 2$ technical replicates and have been performed in at least two biologically independent experiments. GMTs are shown with a color-matched bar (and reported in table S1) with the fold change compared with Wu-G614 indicated above. Demographics of enrolled donors are provided in data S1. (**B**) Cross-reactivity of IgGs secreted from memory B cells obtained from infected-vaccinated individuals ($n = 11$), primary SARS-CoV-2 infected individuals ($n = 3$ samples collected at 1 to 3 months and $n = 2$ samples collected at 6 to 7 months), or breakthrough cases ($n = 7$ samples collected at 1 to 3 months and $n = 4$ samples collected at 4 to 6 months) occurring in January–March 2022, when the prevalence of Omicron BA.1/BA.2 exceeded 90% in the region where samples were obtained (fig. S2). Each dot represents a well containing oligoclonal B cell supernatant screened for the presence of IgGs binding to the SARS-CoV-2 Wuhan-Hu-1 and BA.1 RBDs (top) or to the SARS-CoV-2 Wuhan-Hu-1 and SARS-CoV RBDs (bottom) using ELISA. Red dots indicate inhibition of the interaction with ACE2 (using Wuhan-Hu-1 target antigen) as determined in a separate assay. The percentages are expressed relative to the total positive hits against any of the antigens tested. Numbers of positive hits relative to individual donors are shown in fig. S3. (**C**) Frequency analysis of site-specific IgG antibodies derived from memory B cells. RBD sites targeted by IgG derived from memory B cells were defined by a blockade-of-binding assay using mAbs specific for sites Ia (S2E12), Ib (S2X324), IIa (S2X259), IV (S309; parent of sotrovimab), and V (S2H97). Hybrid sites Ia/Ib, Ia/IIa, Ib/IIa, Ib/IV, IIa/V, and IV/V were defined by competition with the two corresponding mAbs. Hybrid sites exhibiting competition with more than two mAbs are indicated as "multiple." Lack of competition is indicated as "other." Pie charts show cumulative frequencies of IgGs specific for the different sites among total RBD-directed IgG antibodies (left) and those inhibiting binding of RBD to human ACE2 (right) in $n = 11$ infected-vaccinated individuals or $n = 7$ breakthrough cases. (**D**) Neutralizing activity against Wu-G614 and BA.1 S VSV pseudoviruses determined from nasal swabs obtained longitudinally upon BA.1 breakthrough infection up to approximately 180 days after a positive PCR test [post (+) PCR]. (**E**) Neutralizing activity against Wu-G614 and BA.1 S VSV pseudoviruses from nasal swabs obtained longitudinally after a negative PCR test [post (–) PCR)] in vaccinated-only individuals.

to exposure to BA.1 S because no correlation was found between time intervals and GMTs (data S1). Neutralizing GMTs against the SARS-CoV S pseudovirus was reduced for all cohorts by 8.6- to 25-fold relative to Wu-G614 S VSV, underscoring the marked genetic and antigenic divergence of this sarbecovirus clade (*19*, *27*, *28*).

Given the recall of Wuhan-Hu-1 plasma-neutralizing antibodies in Omicron breakthrough cases, we investigated the cross-reactivity of RBD-directed antibodies produced by in vitro–stimulated memory B cells obtained up to 200 days after infection or vaccination, as well as in circulating plasma cells collected in the days after infection (*29*). These analyses used blood samples from individuals who were infected before the emergence of Omicron and subsequently vaccinated ("infected-vaccinated 2/3 doses"), as well as subjects who experienced either an Omicron primary infection or an Omicron breakthrough infection. Primary and breakthrough Omicron infections occurred between January and March 2022, during which time the prevalence of Omicron BA.1/BA.2 sublineages exceeded 90% in the region from which the samples were obtained (fig. S2). Plasma-neutralizing activity of Omicron-infected (primary and breakthrough) cases was reduced an average of 6.1-fold against BA.4/BA.5 S VSV relative to BA.1 S VSV (table S2), likely as a result of both RBD and NTD mutations in the former lineage, concurring with the above data and recent studies (*30*, *31*). More than 80% of SARS-CoV-2 RBD-directed IgGs secreted by memory B cells and plasma cells obtained from breakthrough cases cross-reacted with the Wuhan-Hu-1, BA.1, BA.2, BA.4/5 and Delta RBDs, and >90% of these antibodies blocked binding to ACE2 [a correlate of neutralization (*13*, *32*)] (Fig. 1B, figs. S3 to S6, and table S2). Moreover, Omicron breakthrough infections failed to elicit BA.1-, BA.2-, or BA.4/5-specific RBD-directed memory B cells. Notably, a fraction of RBD-directed antibodies (7 to 9%) cross-reacted with the Wuhan-Hu-1 and BA.2 RBDs but not with the BA.1 RBD, and a smaller fraction (1 to 3%) also cross-reacted with the Wuhan-Hu-1 and BA.4/5 RBDs but not with the BA.1 RBD, consistent with the antigenic distance of BA.1 from the other Omicron sublineages (Fig. 1B, figs. S3 to S6, and table S2). Furthermore, the proportion of BA.4/5-reacting antibodies cross-reacting with Wuhan-Hu-1, BA.1, and BA.2 decreased over time when comparing 1 to 3 months versus 4 to 6 months after breakthrough infections (fig. S4, D to F). This suggests that the maturation of antibodies driven by BA.1 or BA.2 breakthrough infections may also result in a narrowing of their specificity over time, thereby decreasing cross-reactivity with the BA.4/5 RBD. These findings illustrate how immunological imprinting from prior exposure, also referred to as "original antigenic sin," can strongly affect the response to distantly related antigens. By contrast, memory B cell–derived RBD-directed IgG antibodies obtained from Omicron primary infections up to 6 to 7 months after infection were present at low frequency and were mostly specific for the BA.1 and BA.2 RBDs, (Fig. 1B, figs. S3 to S6, and data S1). The frequency of IgG antibodies cross-reacting with the SARS-CoV RBD was similar across all three cohorts, concurring with the overall weak plasma-neutralizing activity (Fig. 1, A and B, and table S2).

We determined the site specificity of RBD-directed antibodies secreted by stimulated memory B cells by competition with structurally characterized mAbs targeting four distinct antigenic sites (*13*, *27*). Most of the memory B cell–derived antibodies from (pre-Omicron) infected-vaccinated individuals competed with the five reference mAbs used, whereas a large fraction of antibodies from Omicron breakthrough cases did not compete with any of these five mAbs, indicating that they recognize other undefined RBD antigenic sites (Fig. 1C and fig. S7). Antibodies recognizing most antigenic sites overlapping with the receptor-binding motif (RBM), such as mAb S2E12 (*33*), were found at lower frequency upon Omicron breakthrough infections relative to infected-vaccinated subjects, consistent with the presence of several immune escape mutations in the Omicron RBM (Fig. 1C and fig. S7) (*3*, *18*). A similar relative reduction was observed for antibodies targeting RBD antigenic site IIa [recognized by the S2X259 mAb (*34*)] (Fig. 1C and fig. S7), in agreement with previous findings describing Omicron immune escape from several site IIa mAbs (*3*, *8*, *18*). Collectively, these findings demonstrate that Omicron breakthrough infections preferentially expand existing B cell pools primed by vaccination and elicit cross-reactive antibodies, supporting the concept of immunological imprinting.

To evaluate mucosal antibody responses in subjects who experienced a BA.1 breakthrough infection or in vaccinated-only subjects, we assessed IgG- and IgA-binding titers in nasal swabs obtained longitudinally after polymerase chain reaction (PCR) testing. Although we detected S-specific IgG, and to a lesser extent IgA, in swabs from several breakthrough cases, vaccinated-only individuals had no detectable binding antibody titers (fig. S8, A to D, and fig. S9, A and B). Accordingly, we observed mucosal neutralizing activity against Wu-G614 and BA.1 S VSV pseudoviruses for nasal swabs obtained from breakthrough cases throughout the month after symptom onset, corresponding to up to 19 days after positive PCR testing (Fig. 1, D to E; fig. S9C; and data S1). Furthermore, analysis of nasal swabs obtained from four breakthrough cases ~6 months after symptom onset demonstrated a retention of neutralizing activity.

Assessing plasma-neutralizing antibody titers of these BA.1 breakthrough cases yielded similar magnitude and GMT reductions compared with the rest of the BA.1 breakthrough cohort (Fig. 1A, fig. S1F, and data S1). The magnitude of the neutralizing antibody responses in nasal swabs cannot be directly compared with plasma samples because of the self-administration procedure and resulting sample nonuniformity. Overall, we observed heterogeneous mucosal neutralizing antibody responses among BA.1 breakthrough cases but not in vaccinated-only individuals (Fig. 1, D and E; fig. S9, C and D; and data S1). Collectively, these data underscore the lack of or very weak induction of mucosal antibody responses upon intramuscular delivery of mRNA vaccines or adenovirus-vectored vaccines (*35*, *36*) and are consistent with concurrent findings that Omicron breakthrough infection, but not vaccination alone, induces neutralizing antibody responses and tissue-resident T cells in the nasal mucosa (*37*, *38*).

Omicron sublineages escape neutralization mediated by most clinical mAbs

We next evaluated the impact of BA.1, BA.2, BA.3, BA.4, BA.5, BA.2.12.1, and BA.2.75 S mutations on neutralization mediated by a panel of RBD-directed mAbs using VSV pseudoviruses and VeroE6 target cells. The site Ib COV2-2130 mAb weakly neutralized BA.1 (*3*), whereas it neutralized BA.2, BA.3, BA.4, BA.5, BA.2.12.1, and BA.2.75 S VSV pseudoviruses with 1.6-, 4.2-, 14.5-, 8.8-, 2.0-, and 7.9-fold decreases, respectively, in half-maximal inhibition concentration (IC_{50}) compared with Wu-D614 S VSV (Fig. 2A and fig. S10, A and B). Moreover, the COV2-2196 + COV2-2130 mAb cocktail had 106.4-, 7.6-, 35-, 92.8-, 46.5-, 9.3-, and 9.1-fold decreases in potency against BA.1, BA.2, BA.3, BA.4, BA.5, BA.2.12.1, and BA.2.75, respectively (Fig. 2A and fig. S10, A and B). Because COV2-2196 weakly inhibited Omicron sublineages (except for BA.2.75, for which the reduction in IC_{50} was 17.3-fold), the neutralizing activity of the cocktail was largely mediated by COV2-2130. Within the COV2-2130 epitope, position 446 is a glycine residue for Wuhan-Hu-1, BA.2, BA.4, BA.5, and BA.2.12.1 S or a serine residue in BA.1, BA.3, and BA.2.75 S, the latter residue disrupting the binding interface of COV2-2130 (*18*). The importance of this site was also identified through deep mutational scanning (*39*), and this point mutation was shown to reduce neutralizing activity by ~4-fold for COV2-2130 (*8*). The greater reduction in potency against BA.4 and BA.5 relative to BA.2 is likely driven by the L452R mutation, as reported (https://www.fda.gov/media/154701/download) (*39*). The REGN10987 + REGN10933 and LY-CoV16 + LY-CoV555 mAb cocktails and the CT-P59 and ADI-58125 mAbs had reductions of in vitro neutralization potency ranging between two and four orders of magnitude against all Omicron sublineage S VSV pseudoviruses compared with Wu-D614 S VSV because of mutations in the RBM (Fig. 2A and fig. S10, A and B) (*18*). CT-P59, however, retained neutralizing activity against the BA.2.75 sublineage (29.2-fold reduction relative to Wu-D614 S VSV). The recently described ACE2-mimicking S2K146 mAb (*40*), which retained unaltered activity against BA.1 compared with Wu-D614 (*3*), had a mildly reduced neutralizing activity against BA.2, BA.3, BA.2.12.1, and BA.2.75 S VSV pseudoviruses (3.3-, 3.1-, 1.9-, and 4.3-fold, respectively) (Fig. 2A and fig. S10, A and B). However, S2K146 had a marked reduction in neutralizing activity against BA.4 and BA.5 (with 472- and 285-fold IC_{50} reductions compared with Wu-D614 S VSV), likely caused by the F486V mutation.

Sotrovimab, a site IV mAb with broad sarbecovirus (clade Ia and Ib) cross-neutralizing activity (*41*), had a 16-, 7.3-, 21.3-, 22.6-, 16.6-, and 8.3-fold reduction in potency relative to Wu-D614 against VSV pseudoviruses expressing BA.2, BA.3, BA.4, BA.5, BA.2.12.1, and BA.2.75 S proteins, respectively (Fig. 2A). Similar reductions in neutralizing activity were also observed against authentic Omicron sub-lineage virus isolates (Fig. 2C and fig. S11), and are greater than that observed against BA.1 pseudovirus (2.7-fold), although no additional residue mutations map to the sotrovimab epitope except the G339H substitution present in BA.2.75 instead of G339D found in BA.1 (*41*–*43*). We recently showed that sotrovimab retained in vitro effector functions against BA.2 and conferred Fc-dependent protection in the lungs of mice infected with BA.2 (*44*). The additional loss of neutralization of these Omicron sublineage VSV pseudoviruses beyond BA.1 likely results from the S371F substitution, which is found in BA.2, BA.3, BA.4/5, BA.2.12.1, and BA.2.75, and introduces a bulky phenylalanine near the N343 glycan, which is part of the sotrovimab epitope (*41*). A recently determined BA.2 S structure shows that the RBD helix comprising residues 364 to 372 is indeed remodeled (*45*) and adopts a distinct conformation from the ones observed for Wuhan-Hu-1 S or BA.1 S structures (*18*, *46*). This structural rearrangement is sterically incompatible with the glycan N343 conformation observed in S309-bound spike structures (*18*, *41*), as supported by molecular dynamics simulations, and likely explains the reductions in neutralization potency (fig. S11, A to D). Although we could not test the effect of the S371F substitution alone in the Wu-D614 S background (because of poor VSV pseudovirus infectivity), the S371F, S373P, S375F, and D614G mutant (as found in BA.2, BA.3, BA.4, BA.5, BA.2.12.1, and BA.2.75) reduced sotrovimab-mediated neutralization by 3.4-fold relative to Wu-D614 S VSV (fig. S11E and table S3). Moreover, the S371L, S373P, and S375F triple mutant (as found in BA.1) did not alter sotrovimab activity (fig. S11F and table S3), lending further support to the role of F371 in reducing the sotrovimab potency against BA.2, BA.3, BA.4, BA.5, BA.2.12.1, and BA.2.75.

S2X259, a site IIa mAb that broadly reacts with the RBD of multiple sarbecoviruses (*34*), retained activity against BA.1 (*3*). However, the neutralization potency of S2X259 was decreased by one to two orders of magnitude against BA.2, BA.3, BA.4, BA.5, BA.2.12.1, and BA.2.75 S VSV pseudoviruses (Fig. 2A and fig. S10, A and B), likely because of the detrimental effect of the aforementioned S371F/S373P/S375F–induced remodeling and of the R408S mutation (*34*). S2H97 is a site V mAb that had a 4.7- to 10-fold decrease in neutralization potency against Omicron sublineages compared with Wu-D614 S VSV (Fig. 2A and fig. S10, A and B) despite the absence of mutations present in the epitope or otherwise found to affect binding by DMS, perhaps reflecting differential accessibility to its cryptic epitope in the context of these S trimers (*27*).

Identification of the pan-variant and ultrapotent neutralizing mAb S2X324

The S2X324 mAb stood out in our panel because its neutralization potency was largely unaffected by the BA.1, BA.2, BA.3, BA.4, BA.5, BA.2.12.1, and BA.2.75 S mutations (Fig. 2A and fig. S10, A and B). S2X324 cross-reacted with and neutralized all SARS-CoV-2 (VSV pseudovirus and authentic virus) variants tested, with IC_{50} values <10 ng/ml except BA.2.75, for which the IC_{50} was 18 ng/ml (Fig. 2, B and C; figs. S10, A to C, S12, and S13; and table S4). S2X324 cross-reacted with the sarbecovirus clade 1b Pangolin-GD RBD but did not recognize more divergent sarbecovirus RBDs (Fig. 2D), in contrast to the previously described broadly neutralizing mAb S2X259 (*34*). Furthermore, S2X324 inhibited binding of the SARS-CoV-2 RBD to human ACE2 in a concentration-dependent manner, as measured by competition enzyme-linked immunosorbent assay (ELISA) (Fig. 2E), and induced slow, premature shedding (*47*) of the S_1 subunit from cell surface–expressed S (Fig. 2F). However, S2X324 did not promote the fusogenic conformational changes of a wild-type–like purified recombinant S ectodomain trimer (fig. S14), likely because of the slow kinetics of S_1 shedding. This suggests that blockage of ACE2 binding is the main mechanism of S2X324-mediated inhibition of SARS-CoV-2.

To evaluate the ability of S2X324 to promote antibody dependent-phagocytosis or cytotoxicity, we tested whether the mAb could activate Fcγ receptors expressed at the surface of Jurkat cells. Although S2X324 only activated FcγRIIIa, but not FcγRIIa, in vitro (fig. S15, A and B), it triggered both antibody-dependent phagocytosis and cytotoxicity after incubation of

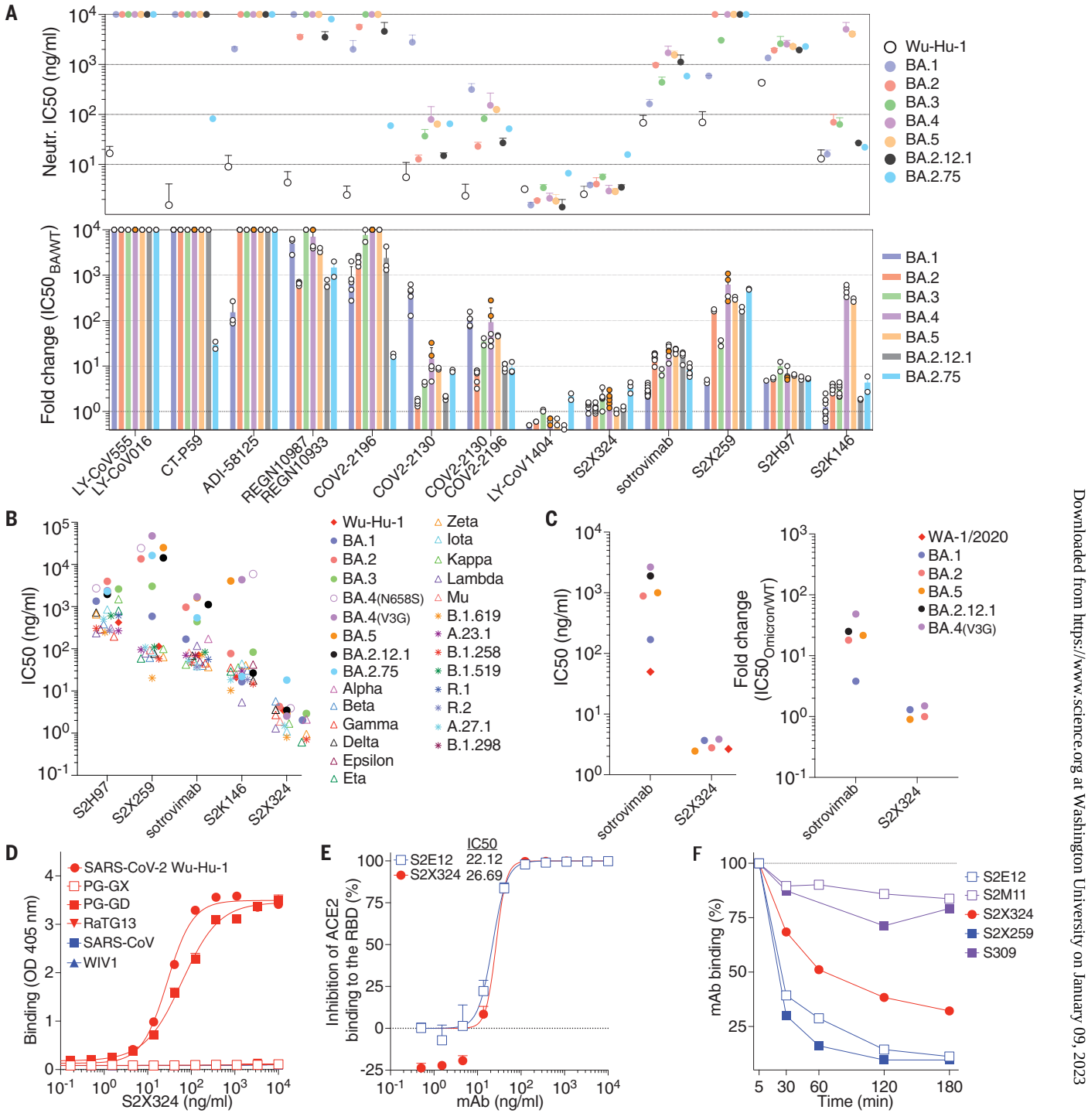

Fig. 2. Identification and characterization of S2X324 as a pan-variant RBD-directed mAb. (**A**) mAb-mediated neutralization of BA.1, BA.2, BA.3, BA.4, BA.5, BA.2.12.1, and BA.2.75 S VSV pseudoviruses. Two haplotypes of BA.4 S were tested: BA.4-V3G (orange dots) and BA.4-N658S (white dots), and the IC_{50} values reported in the text are the averages of both haplotypes. The potency of each mAb or mAb cocktail is represented by their IC_{50} (top, geometric mean ± SD) or fold change relative to neutralization of the Wuhan-Hu-1 (D614) pseudovirus (bottom, average ± SD). (**B**) Neutralization of SARS-CoV-2 variant S VSV pseudoviruses mediated by broadly neutralizing mAbs. Each symbol represents the GMT of at least two independent experiments. (**C**) Neutralizing activity (left) and fold change relative to WA-1/2020 (right) of S2X324 and sotrovimab against SARS-CoV-2 Omicron BA.1, BA.2, BA.4, BA.5, and BA.2.12.1 authentic viruses using VeroE6-TMPRSS2 target cells. Data are representative of at least two biological independent experiments. Neutralization of Omicron BA.1 by sotrovimab refers to previously published data (*3*). (**D**) Cross-reactivity of S2X324 with sarbecovirus clade 1a and 1b RBDs analyzed by ELISA. PG-GX, Pangolin-Guangxi; PG-GD, Pangolin-Guangdong. (**E**) Preincubation of serial dilutions of S2X324 or S2E12 with the SARS-CoV-2 RBD prevents binding to the immobilized human ACE2 ectodomain in ELISA. Error bars indicate SD between replicates. (**F**) S2X324-mediated S_1 shedding from cell surface–expressed SARS-CoV-2 S as determined by flow cytometry. S2E12 and S2X259 were used as positive controls, and S2M11 and S309 were used as negative controls.

peripheral blood mononuclear cells with SARS-CoV-2 S-expressing cells (fig. S15, C to F). The slow S_1 shedding kinetics likely explain the ability of S2X324 to promote Fc-mediated effector functions.

Structural basis for S2X324-mediated neutralization

To understand the pan-variant S2X324 inhibitory activity, we determined a cryo–electron microscopy structure of the Omicron BA.1 S ectodomain trimer bound to the S2X324 Fab fragment at 3.1-Å resolution (Fig. 3A, fig. S16, and table S5). In our structure, the BA.1 S trimer had three Fabs bound to one closed and two open RBDs. We used focused classification and local refinement of the closed RBD-S2X324 Fab complex to obtain a 3.3-Å structure revealing the molecular details of the binding interface.

S2X324 recognizes an RBD epitope partially overlapping with antigenic sites Ib and IV (Fig. 3, A and B), explaining the observed competition with the S2H14 (*13*) and S309 (sotrovimab parent) (*41*) mAbs (fig. S13B). S2X324 uses all six complementary-determining loops to recognize RBD residues T345, N439, K440, L441, S443, K444, V445, S446, G447, N448, Y449, N450, R498, P499, T500, Y501, G502, Q506, and R509 (Fig. 3C). Consistent with the competition assay, S2X324 overlaps with the RBM on the RBD and would sterically hinder receptor engagement (Figs. 2E and 3D).

The structure explains how this mAb accommodates residues that are mutated in Omicron lineages relative to Wuhan-Hu-1: N440K (BA.1/BA.2/BA.3/BA.4/BA.5/BA.2.12.1/BA.2.75), G446S (BA.1/BA.3//BA.2.75), Q498R (BA.1/BA.2/BA.3/BA.4/BA.5/BA.2.12.1/BA.2.75), and N501Y (BA.1/BA.2/BA.3/BA.4/BA.5/BA.2.12.1/BA.2.75). Specifically, K440 forms a salt bridge with the VL E53 side chain, S446 forms van der Waals interactions with VH R60 and VL S96/S97, whereas R498 forms electrostatic interactions with the VL S96 backbone. Our structure further suggests that the tighter binding of S2X324 to the Wuhan-Hu-1 and BA.2 RBDs relative to BA.1 (fig. S13A) might be caused by G446S, because although the mutation is clearly accommodated, at least one of three favored rotamers for S446 would clash with the Fab. The Y501 backbone forms van der Waals interactions with the VL N32 side chain that are independent of the RBD residue identity at position 501 (explaining retention of neutralization of all Y501-containing variants). S2X324 and LY-CoV1404 share 87 and 91% amino acid sequence identity in their heavy and light chains, respectively, likely explaining their similar binding mode (fig. S17) (*48*), pan-variant neutralizing activity (*49*), and comparable resilience to Omicron sublineage mutations thus far (Fig. 2A).

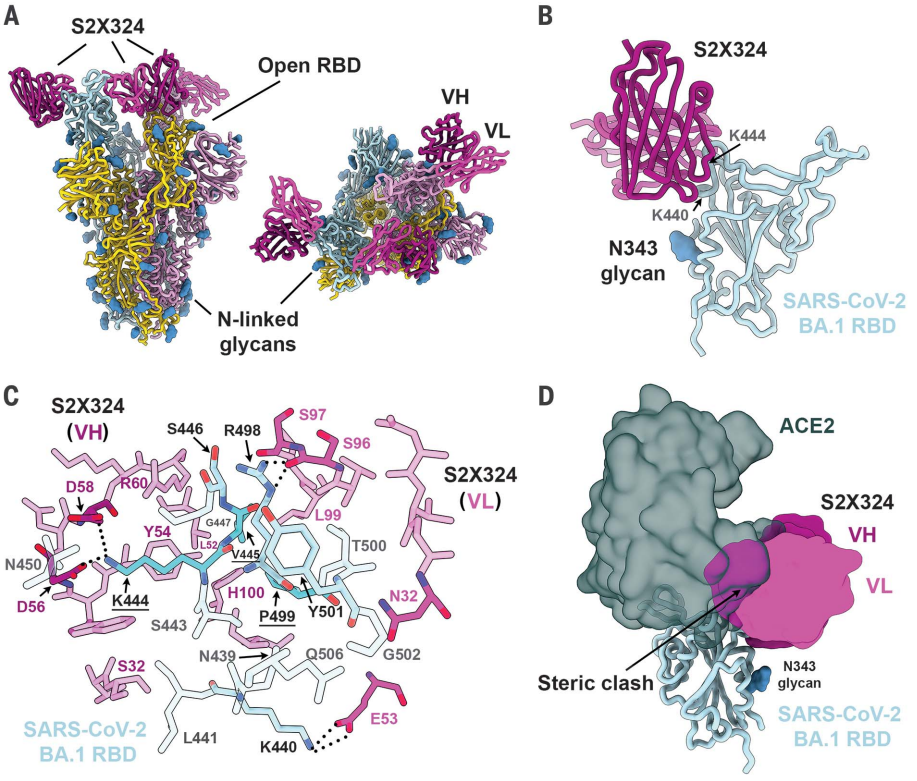

Fig. 3. Structural characterization of the S2X324 pan-variant mAb. (**A**) Cryo-EM structure viewed along two orthogonal orientations of the prefusion SARS-CoV-2 Omicron BA.1 S ectodomain trimer with three S2X324 Fab fragments bound. SARS-CoV-2 S protomers are colored light blue, pink, and gold. S2X324 heavy-chain and light-chain variable domains are colored purple and magenta, respectively. Glycans are shown as blue spheres. (**B**) Ribbon diagram of the S2X324-bound SARS-CoV-2 RBD. The N343 glycan is shown as blue spheres. (**C**) Magnified view of the contacts formed between S2X324 and the SARS-CoV-2 BA.1 RBD. Selected epitope residues are labeled, and electrostatic interactions are indicated with dotted lines. A few of the escape mutants identified are colored turquoise. (**D**) Superimposition of the S2X324-bound (purple and magenta) and ACE2-bound [dark gray, PDB 6M0J (*94*)] SARS-CoV-2 RBD (light blue) structures showing steric overlap. The N343 glycan is shown as blue spheres.

Identification of S2X324 viral escape mutants in vitro

To explore potential mutations that could promote escape from S2X324-mediated neutralization, we passaged a replication-competent VSV chimera harboring either SARS-CoV-2 Wu-G614 S (*50*) or Omicron BA.1 S in the presence of S2X324. Residue substitutions at three distinct sites emerged in both S backgrounds (Fig. 3C; fig. S18, A and B; and tables S6 and S7): (i) K444N/T (Wu-G614 and BA.1 background) and K444E/M (BA.1 background), which would abrogate the salt bridges formed between the K444 side chain and the heavy chain D56 and D58 side chains; (ii) V445D (Wu-G614 background) and V445A/F (BA.1 background), which would disrupt Van der Waals contacts with S2X324; and (iii) P499R (Wu-G614 background) and P499S/H (BA.1 background), which might alter the local RBD backbone conformation and/or sterically hinder mAb binding. Furthermore, three additional mutations were detected in the BA.1 S background only, S446I, G447S, and N448K, which are positioned near the interface between the heavy and light chains (Fig. 3C; fig. S18, A and B; and tables S6 and S7). The VSV chimera harboring SARS-CoV-2 Wu-G614 S outcompeted the chimeras harboring the K444T/N, V445D, or P499R escape mutants after four rounds of passaging, suggesting reduced fitness in this replicating chimeric virus model system (fig. S18C). Even though each of these mutations requires a single nucleotide substitution, they are very rare and have been detected cumulatively only in 0.087 and 0.080% of Delta and Omicron genome sequences as of 12 August 2022, respectively (table S8 and fig. S19), although the frequency of some of them is increasing. We further tested VSV pseudoviruses bearing Wu-G614, BA.1, or BA.2 S carrying K444E, K444D, K444N, K444T, V445D, and P449R/H, and confirmed that these mutations abrogated or strongly reduced S2X324-neutralizing activity (fig. S19 and table S9). In addition, S2X324-neutralizing activity was abrogated when V445T/A/F was introduced in the BA.1 backbone (table S9). S2X324 retained potent neutralizing activity

against pseudoviruses bearing other mutations in the epitope found in known variants such as N439K, N440K, and N501Y in the Wu-G614 S background (table S9). Although the S2X324 escape mutants identified are rare, these data suggest that a mAb cocktail comprising S2X324 would increase the barrier for the emergence of resistance mutants even further compared with this single mAb.

S2X324 protects hamsters against SARS-CoV-2 Delta, BA.2, and BA.5 variants

We investigated the in vivo prophylactic and therapeutic efficacy of S2X324 using Syrian hamsters challenged with SARS-CoV-2 variants. Prophylactic administration of S2X324 or S309 comparably protected hamsters challenged with SARS-CoV-2 Delta in a dose-dependent manner (Fig. 4, A to C) despite a 20-fold difference in in vitro potency against SARS-CoV-2 Delta S VSV (Fig. 2B). These data support the lack of direct correlation between in vitro and in vivo potency that was previously reported (*51*, *52*). Moreover, prophylactic administration of S2X324 at 5 mg/kg decreased viral loads below detection levels in the lungs of hamsters challenged with BA.2 or BA.5 (Fig. 4, D to F). In this model, S309 retained activity against BA.5 despite a 22.6-fold reduced in vitro potency relative to Wu-D614 (Fig. 2, A and B). Therapeutic administration of hamster IgG2a S2X324 (1 day after challenge with the SARS-CoV-2 Delta variant) at 2 and 5 mg/kg prevented body weight loss and reduced lung viral RNA loads by 2.5 and 3 orders of magnitude compared with the control group, respectively (Fig. 4, G and H). Viral replication in the lungs was fully abrogated at 2 and 5 mg/kg of S2X324 and reduced by about one order of magnitude for animals treated with 0.1 and 0.5 mg/kg of S2X324 (Fig. 4I). No statistically significant differences were observed for animals receiving an Fc-silenced version of S2X324 (N297A) versus the groups receiving the same doses of Fc-competent S2X324, indicating that limited contribution of Fc-mediated effector functions in these experimental conditions.

Discussion

Immune imprinting, which is also referred to as original antigenic sin, was described based

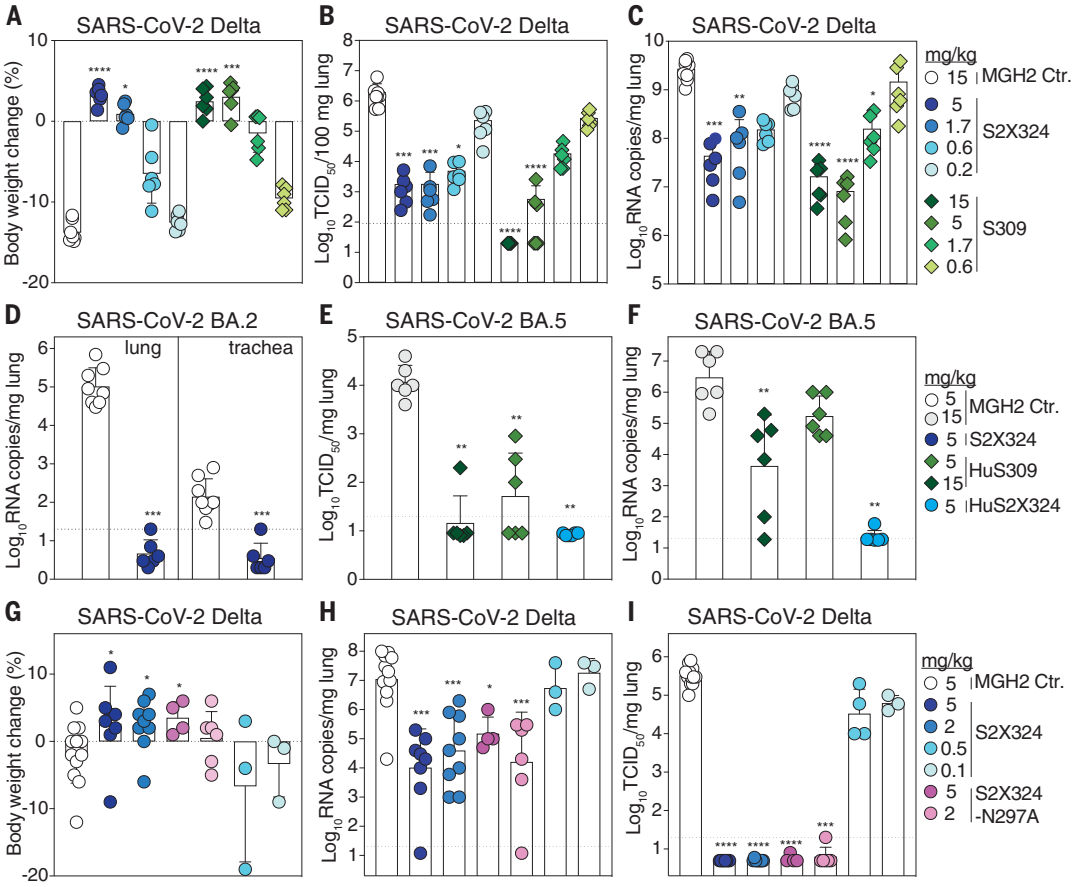

Fig. 4. S2X324 protects hamsters against SARS-CoV-2 Delta, BA.2, and BA.5 challenge. (**A** to **C**) Dose-dependent (expressed in milligrams of mAb per kilogram of body weight) prophylactic protection of S2X324 (blue circles) and S309 (green diamonds) hamster IgG2a (harboring hamster IgG2a constant regions) administered to animals 1 day before infection with SARS-CoV-2 Delta. Animals were evaluated 4 days after infection on the basis of the fraction of body weight change (A), replicating viral titers [50% tissue culture infectious dose ($TCID_{50}$)] (B), and viral RNA load (C). n = 6 animals/dose. *P < 0.05, **P < 0.01, ***P < 0.001, and ****P < 0.0001 relative to isotype control (MGH2 mAb against circumsporozoite protein of Plasmodium sporozoites). Data were analyzed with Kruskal-Wallis test followed by Dunn's multiple-comparisons test. (**D**) Quantification of viral RNA loads in the lung and trachea of Syrian hamsters 4 days after intranasal infection with SARS-CoV-2 Omicron BA.2, which was preceded 1 day prior by prophylactic intraperitoneal administration of S2X324 hamster IgG2a at 5 mg/kg of body weight. ***P < 0.001 relative to control. Data were analyzed with Mann-Whitney two-tailed t test. (**E** and **F**) Quantification of replicating virus titers ($TCID_{50}$) (E) and viral RNA load (F) in the lung of Syrian hamsters 4 days after intranasal infection with SARS-CoV-2 Omicron BA.5, which was preceded 1 day prior by prophylactic intraperitoneal administration of S309 or S2X324 human IgG1 (HuS309 and HuS2X324). (**G** to **I**) Dose-dependent protection in animals 4 days after infection with SARS-CoV-2 Delta by therapeutic intraperitoneal administration of S2X324 hamster IgG2a (blue symbols) or the S2X324 N297A mutant IgG2a (purple symbols) 1 day later at 5, 2, 0.5, or 0.1 mg/kg of body weight. *P < 0.05, **P < 0.01, ***P < 0.001, and ****P < 0.0001 relative to control, respectively. Data were analyzed with Mann-Whitney two-tailed t test.

on the observation that infections with influenza virus strains distinct from the one that caused prior infection preferentially boosted antibody responses against epitopes shared with the original strain (*53*). Although this phenomenon is often considered detrimental, it can also be beneficial, as was the case at the time of the 2009 H1N1 pandemic, during which initial antibody responses to infection with this newly emerged and antigenically shifted virus were dominated by antibodies targeting the conserved hemagglutinin stem region (*54*, *55*). Subsequent exposures through vaccination or infection elicited antibody responses to the shifted variant (i.e., to "non-conserved" hemagglutinin epitopes) (*54*, *56*). Moreover, several studies reported hemagglutinin stem-directed antibody-mediated protection against H5N1 and H7N9 zoonotic influenza strains through imprinting during childhood resulting from exposure to seasonal H1N1 and H3N2, respectively (*55*, *57*). Similarly, we show that exposure to antigenically shifted Omicron strains primarily recalls existing memory B cells specific for epitopes shared by multiple SARS-CoV-2 variants rather than priming naïve B cells recognizing Omicron-specific epitopes (at least up to 180 days after breakthrough infection), as was also recently reported (*58*). Although immune imprinting may be beneficial for stimulating responses to cross-reactive SARS-CoV-2 S epitopes, antibody responses to some Omicron S-specific epitopes were hindered by prior antigenic exposure.

Currently, there is uncertainty whether vaccines matching dominant circulating SARS-CoV-2 variants such as those used for seasonal influenza are needed, or if the repeated use of Wuhan-Hu-1–based vaccines will suffice. Recent work showed that boosting previously immunized macaques with Beta or Omicron mRNA S vaccines or with Beta RBD nanoparticle vaccines elicited comparably high titers of antibodies broadly neutralizing multiple variants relative to Wuhan-Hu-1–based vaccines (*59*–*61*). Furthermore, administration of Wuhan-Hu-1–based vaccine boosters in humans was shown to elicit appreciable titers of neutralizing antibodies and prevent severe disease associated with Omicron infections (*11*, *19*, *62*–*65*). The limited cross-variant neutralization elicited by Omicron primary infection in humans or Omicron-based vaccination of immunologically naïve animals and the data on the specificity of memory B cells presented here indicate that an Omicron-based vaccine might elicit antibody responses directed toward the vaccine-matched and closely related antigens. This suggests that a heterologous prime boost or a multivalent approach might be preferable (*59*, *66*–*73*). Omicron infection and Omicron S-based vaccination of previously immune subjects, however, recalls cross-reactive memory B cells (*58*, *74*), which may further mature over time to enhance their affinity and neutralizing potency against Omicron, but also to possibly broaden their neutralizing activity against past and future variants. Indeed, multiple studies have shown that somatic hypermutations yield RBD-specific mAbs with increased affinity for the homotypic antigen and augmented resilience to immune evasion of emerging heterotypic variants (*40*, *75*–*79*). The recently introduced bivalent mRNA vaccine boosters encoding the Wuhan-Hu-1 and either the BA.1 or the BA.4/5 S glycoproteins have yielded encouraging results (*80*–*82*).

Understanding antibody responses elicited by and directed toward Omicron sublineages is as the result of key to informing public health policies and the design of SARS-CoV-2 and sarbecovirus vaccines (*70*, *71*, *83*–*85*). Our data show that Omicron breakthrough infections do not elicit high titers of pan-sarbecovirus–neutralizing antibodies (e.g., directed against SARS-CoV), in agreement with recent data (*86*). These findings contrast with the observation that preexisting immunity to SARS-CoV followed by SARS-CoV-2 vaccination is associated with elicitation of pan-sarbecovirus–neutralizing antibodies (*28*). These different outcomes might be explained by the low frequency of memory B cells encoding neutralizing antibodies targeting antigenic sites shared among pre-Omicron variants (Wuhan-Hu-1–related strains), Omicron, and SARS-CoV because of the genetic and antigenic distances between these three distinct viruses. For instance, Omicron BA.1 and BA.2 harbor variations of the RBD antigenic site II, which is the target of pan-sarbecovirus–neutralizing antibodies such as S2X259 (*34*), DH1047 (*87*), and ADG2 (*88*), leading to resistance to the neutralization mediated by some of these mAbs (*3*, *8*, *18*). This suggests that conservation of RBD antigenic sites across sarbecoviruses may have resulted (at least partially) from limited immune pressure rather than from functional or structural constraints (i.e., some mutations at these conserved sites may remain compatible with viral fitness) (*86*).

Recent preclinical assessment of intranasally administered influenza and sarbecovirus vaccine candidates has demonstrated the induction of lung-resident protective mucosal humoral and cellular immunity at the site of viral entry (*89*–*92*). These observations, along with our findings that SARS-CoV-2 breakthrough infections, but not vaccination alone, elicit neutralizing activity in the nasal mucosa, support the development and evaluation of a next generation of vaccines administered intranasally.

REFERENCES AND NOTES

1. R. Viana *et al*., *Nature* **603**, 679–686 (2022).
2. J. Yu *et al*., medRxiv 2022.02.06.22270533 [Preprint] (2022); https://doi.org/10.1101/2022.02.06.22270533.
3. E. Cameroni *et al*., *Nature* **602**, 664–670 (2022).
4. J. E. Bowen *et al*., *Science* **377**, 890–894 (2022).
5. C.-W. Tan *et al*., *Lancet Microbe* S2666-5247(22)00220-8 (2022).
6. P. A. Desingu, K. Nagarajan, K. Dhama, *J. Med. Virol.* **94**, 1808–1810 (2022).
7. H. Tegally *et al*., medRxiv 2022.05.01.22274406 [Preprint] (2022); https://doi.org/10.1101/2022.05.01.22274406.
8. L. Liu *et al*., *Nature* **602**, 676–681 (2022).
9. D. Planas *et al*., *Nature* **602**, 671–675 (2022).
10. M. Hoffmann *et al*., bioRxiv 472286 [Preprint] (2021); https://doi.org/10.1101/2021.12.12.472286.
11. W. F. Garcia-Beltran *et al*., *Cell* **185**, 457–466.e4 (2022).
12. H. Gruell *et al*., bioRxiv 487257 [Preprint] (2022); https://doi.org/10.1101/2022.04.06.487257.
13. L. Piccoli *et al*., *Cell* **183**, 1024–1042.e21 (2020).
14. J. E. Bowen *et al*., bioRxiv 473391 [Preprint] (2021); https://doi.org/10.1101/2021.12.19.473391.
15. L. Stamatatos *et al*., *Science* **372**, eabg9175 (2021).
16. A. J. Greaney *et al*., *Sci. Transl. Med.* **13**, eabi9915 (2021).
17. M. McCallum *et al*., *Cell* **184**, 2332–2347.e16 (2021).
18. M. McCallum *et al*., *Science* **375**, 864–868 (2022).
19. A. C. Walls *et al*., *Cell* **185**, 872–880.e3 (2022).
20. A. Y. Collier *et al*., *Sci. Transl. Med.* **14**, eabn6150 (2022).
21. T. A. Bates *et al*., *JAMA* **327**, 179–181 (2022).
22. P. Mlcochova *et al*., Research Square [Preprint] (2021); https://doi.org/10.21203/rs.3.rs-637724/v1.
23. M. McCallum *et al*., *Science* **374**, 1621–1626 (2021).
24. R. Suzuki *et al*., *Nature* **603**, 700–705 (2022).
25. P. Mlcochova *et al*., *Nature* **599**, 114–119 (2021).
26. S. Crotty, *Science* **372**, 1392–1393 (2021).
27. T. N. Starr *et al*., *Nature* **597**, 97–102 (2021).
28. C.-W. Tan *et al*., *N. Engl. J. Med.* **385**, 1401–1406 (2021).
29. D. Pinna, D. Corti, D. Jarrossay, F. Sallusto, A. Lanzavecchia, *Eur. J. Immunol.* **39**, 1260–1270 (2009).
30. K. Khan *et al*., medRxiv 2022.04.29.22274477 [Preprint] (2022).
31. A. Muik *et al*., bioRxiv 502461 [Preprint] (2022); https://doi.org/10.1101/2022.08.02.502461.
32. C. W. Tan *et al*., *Nat. Biotechnol.* **38**, 1073–1078 (2020).
33. M. A. Tortorici *et al*., *Science* **370**, 950–957 (2020).
34. M. A. Tortorici *et al*., *Nature* **597**, 103–108 (2021).
35. L. Azzi *et al*., *EBioMedicine* **75**, 103788 (2022).
36. J. Tang *et al*., *Sci. Immunol.* **7**, eadd4853 (2022).
37. D. Planas *et al*., medRxiv 2022.07.22.22277885 [Preprint] (2022); https://doi.org/10.1101/2022.07.22.22277885.
38. J. M. E. Lim *et al*., *J. Exp. Med.* **219**, e20220780 (2022).
39. J. Dong *et al*., *Nat. Microbiol.* **6**, 1233–1244 (2021).
40. Y.-J. Park *et al*., *Science* **375**, 449–454 (2022).
41. D. Pinto *et al*., *Nature* **583**, 290–295 (2020).
42. E. Cameroni *et al*., bioRxiv 472269 [Preprint] (2021); https://doi.org/10.1101/2021.12.12.472269.
43. A. L. Cathcart *et al*., bioRxiv 434607 [Preprint] (2021); https://doi.org/10.1101/2021.03.09.434607.
44. J. B. Case *et al*., *Nat. Commun.* **13**, 3824 (2022).
45. V. Stalls *et al*., *Cell Rep.* **39**, 111009 (2022).
46. A. C. Walls *et al*., *Cell* **181**, 281–292.e6 (2020).
47. A. C. Walls *et al*., *Cell* **176**, 1026–1039.e15 (2019).
48. K. Westendorf *et al*., bioRxiv 442182 [Preprint] (2022); https://doi.org/10.1101/2021.04.30.442182.
49. K. Westendorf *et al*., *Cell Rep.* **39**, 110812 (2022).
50. J. B. Case *et al*., *Cell Host Microbe* **28**, 475–485.e5 (2020).
51. A. Schäfer *et al*., *J. Exp. Med.* **218**, e20201993 (2021).
52. J. B. Case *et al*., bioRxiv 484787 [Preprint] (2022); https://doi.org/10.1101/2022.03.17.484787.
53. T. Francis, *Proc. Am. Philos. Soc.* **104**, 572–578 (1960).
54. D. Corti *et al*., *Science* **333**, 850–856 (2011).
55. J. Wrammert *et al*., *J. Exp. Med.* **208**, 181–193 (2011).
56. C. S.-F. Cheung *et al*., *Cell Rep.* **32**, 108088 (2020).
57. K. M. Gostic, M. Ambrose, M. Worobey, J. O. Lloyd-Smith, *Science* **354**, 722–726 (2016).
58. J. Quandt *et al*., *Sci. Immunol.* **7**, eabq2427 (2022).
59. M. Gagne *et al*., *Cell* **185**, 1556–1571.e18 (2022).
60. K. S. Corbett *et al*., *Science* **374**, 1343–1353 (2021).
61. P. S. Arunachalam *et al*., *Sci. Transl. Med.* **14**, eabq4130 (2022).
62. E. K. Accorsi *et al*., *JAMA* **327**, 639–651 (2022).
63. H. F. Tseng *et al*., *Nat. Med.* **28**, 1063–1071 (2022).
64. R. Pajon *et al*., *N. Engl. J. Med.* **386**, 1088–1091 (2022).
65. J. E. Bowen *et al*., bioRxiv 484542 [Preprint] (2022); https://doi.org/10.1101/2022.03.15.484542.
66. A. Rössler, L. Knabl, D. von Laer, J. Kimpel, *N. Engl. J. Med.* **386**, 1764–1766 (2022).
67. I.-J. Lee *et al*., bioRxiv 478406 [Preprint] (2022); https://doi.org/10.1101/2022.01.31.478406.
68. S. I. Richardson *et al*., *Cell Host Microbe* **30**, 880–886.e4 (2022).

69. K. Stiasny *et al*., Research Square [Preprint] (2022); https://doi.org/10.21203/rs.3.rs-1536794/v1.
70. A. C. Walls *et al*., *Cell* **184**, 5432–5447.e16 (2021).
71. A. A. Cohen *et al*., *Science* **371**, 735–741 (2021).
72. S. Chalkias *et al*., Research Square [Preprint] (2022); https://doi.org/10.21203/rs.3.rs-1555201/v1.
73. S. S. M. Cheng *et al*., *J. Clin. Virol.* **156**, 105273 (2022).
74. W. B. Alsoussi *et al*., bioRxiv 509040 [Preprint] (2022); https://doi.org/10.1101/2022.09.22.509040.
75. C. Gaebler *et al*., *Nature* **591**, 639–644 (2021).
76. Z. Wang *et al*., *Nature* **595**, 426–431 (2021).
77. D. Pinto *et al*., *Science* **373**, 1109–1116 (2021).
78. J. S. Low *et al*., bioRxiv 486377 [Preprint] (2022); https://doi.org/10.1101/2022.03.30.486377.
79. R. Marzi *et al*., bioRxiv 509852 [Preprint] (2022); https://doi.org/10.1101/2022.09.30.509852.
80. S. Chalkias *et al*., *N. Engl. J. Med.* **387**, 1279–1291 (2022).
81. S. M. Scheaffer *et al*., bioRxiv 507614 [Preprint] (2022); https://doi.org/10.1101/2022.09.12.507614.
82. A. Muik *et al*., bioRxiv 508818 [Preprint] (2022); https://doi.org/10.1101/2022.09.21.508818.
83. A. A. Cohen *et al*., bioRxiv 485875 [Preprint] (2022); https://doi.org/10.1101/2022.03.25.485875.
84. D. R. Martinez *et al*., *Science* **373**, 991–998 (2021).
85. D. Li *et al*., bioRxiv 477915 (2022); https://doi.org/10.1101/2022.01.26.477915.
86. L.-F. Wang *et al*., Research Square [Preprint] (2022); https://doi.org/10.21203/rs.3.rs-1362541/v1.
87. D. R. Martinez *et al*., *Sci. Transl. Med.* **14**, eabj7125 (2022).
88. C. G. Rappazzo *et al*., *Science* **371**, 823–829 (2021).
89. T. Mao *et al*., bioRxiv 477597 [Preprint] (2022); https://doi.org/10.1101/2022.01.24.477597.
90. J. E. Oh *et al*., *Sci. Immunol.* **6**, eabj5129 (2021).
91. S. N. Langel *et al*., *Sci. Transl. Med.* **14**, eabn6868 (2022).
92. A. O. Hassan *et al*., *Cell Rep. Med.* **2**, 100230 (2021).
93. F. A. Lempp *et al*., *Nature* **598**, 342–347 (2021).
94. J. Lan *et al*., *Nature* **581**, 215–220 (2020).

ACKNOWLEDGMENTS

We thank A. E. Powell and N. Czudnochowski for assistance with protein production. **Funding:** This study was supported by the National Institute of Allergy and Infectious Diseases (grants DP1AI158186 and HHSN75N93022C00036 to D.V.), a Pew Biomedical Scholars Award (D.V.), an Investigators in the Pathogenesis of Infectious Disease Award from the Burroughs Wellcome Fund (D.V.), Fast Grants (D.V.), the University of Washington Arnold and Mabel Beckman cryoEM center (D.V.), and the National Institutes of Health (grant S10OD032290 to D.V. and grant AI163019 to S.P.J.W.) D.V. is an Investigator of the Howard Hughes Medical Institute. O.G. is funded by the Swiss Kidney Foundation. **Author contributions:** A.C.W., A.L., D.P., D.C., M.S.P., and D.V. designed the experiments. A.C.W., A.D.M., D.P., C.S., W.R., K.R.S. F.Z., H.V.D., M.G., G.Sc., and F.A.L. isolated mAb and performed binding, neutralization assays, biolayer interferometry, and surface plasmon resonance binding measurements. A.R., J.Z., N.F., M.M.R., and J.N. performed neutralization assays using authentic virus. H.K. confirmed the Spike mutations of authentic virus by Sanger sequencing. A.D.M. and D.P. performed ACE2 binding inhibition and S_1 shedding assays. B.G. and M.A.S. evaluated effector functions. C.S.F., J.B., and L.P performed memory B cell repertoire analysis. O.G., A.C., and P.F. contributed to the recruitment of donors and the collection of plasma samples. J.d.I., L.S., and A.T. performed bioinformatic and epidemiology analyses. Z.L. and S.P.J.W. performed mutant selection and fitness assays. R.A., J.J., F.B., P.M., J.N., G.D.d.M., L.K., and H.B. performed hamster model experiments and data analysis. A.A. performed the EM refolding experiments Y.J.P. prepared cryoEM specimens and collected and processed data collection. Y.J.P. and D.V. built and refined the atomic models. J.E.B. and C.S. purified recombinant glycoproteins. A.L., D.P., Y.J.P., A.D.M., Z.L., D.P., D.C., M.S.P., and D.V. analyzed the data. A.C.W., D.P., D.C., M.S.P., and D.V. wrote the manuscript with input from all authors. F.B., G.S., J.N., S.P.J.W., H.W.V, M.S.P., D.C., and D.V. supervised the project. **Competing interests:** D.P., A.D.M., F.Z., M.G., C.S.F., J.B., C.S., H.V.D., K.H., W.R., M.A.S., G.Sc., B.G., F.B., J.d.I., A.R., J.Z., N.F., H.K., M.M.R, J.N., F.A.L., G.S., L.P., A.T., H.W.V., A.L., M.S.P., and D.C. are employees of Vir Biotechnology Inc. and may hold shares in Vir Biotechnology Inc. L.A.P. is a former employee and shareholder in Regeneron Pharmaceuticals. Regeneron provided no funding for this work. H.W.V. is a founder and holds shares in PierianDx and Casma Therapeutics. Neither company provided resources. D.C. is currently listed as an inventor on multiple patent applications, which disclose the subject matter described in this manuscript. The Veesler laboratory has received a sponsored research agreement from Vir Biotechnology Inc. S.P.J.W. has licensing agreements with Vir Biotechnology and Merck and is a consultant for Thylacine Bio. The remaining authors declare no competing interests. **Data and materials availability:** The cryoEM map and coordinates have been deposited to the Electron Microscopy Databank (SARS-CoV-2 S/S2X324: EMD-28559; SARS-CoV-2 S/S2x324: EMD-28558) and the Protein Data Bank (SARS-CoV-2 S/S2X324: PDB 8ERR; SARS-CoV-2 S/S2x324: PDB 8ERQ). Materials generated in this study will be made available on request, but may require a completed materials transfer agreement signed with Vir Biotechnology Inc. or the University of Washington.

SUPPLEMENTARY MATERIALS

science.org/doi/10.1126/science.adc9127
Materials and Methods
Figs. S1 to S18
Tables S1 to S9
References (*95–126*)
MDAR Reproducibility Checklist
Data S1

View/request a protocol for this paper from *Bio-protocol*.

Submitted 9 May 2022; accepted 17 October 2022
10.1126/science.adc9127

Science

Imprinted antibody responses against SARS-CoV-2 Omicron sublineages

Young-Jun ParkDora PintoAlexandra C. WallsZhuoming LiuAnna De MarcoFabio BenigniFabrizia ZattaChiara Silacci-FregniJessica BassiKaitlin R. SprouseAmin AddetiaJohn E. BowenCameron StewartMartina GiurdanellaChristian SalibaBarbara GuarinoMichael A. SchmidNicholas M. FrankoJennifer K. LogueHa V. DangKevin HauserJulia di IulioWilliam RiveraGretja SchnellAnushka RajeshJiayi ZhouNisar FarhatHannah KaiserMartin Montiel-RuizJulia NoackFlorian A. LemppJavier JanerRana AbdelnabiPiet MaesPaolo FerrariAlessandro CeschiOlivier GianniniGuilherme Dias de MeloLauriane KergoatHervé BourhyJohan NeytsLeah SoriagaLisa A. PurcellGyorgy SnellSean P.J. WhelanAntonio LanzavecchiaHerbert W. VirginLuca PiccoliHelen Y. ChuMatteo Samuele PizzutoDavide CortiDavid Veesler

Science, 378 (6620), • DOI: 10.1126/science.adc9127

Defending against Omicron

The Omicron BA.1 lineage of severe acute respiratory syndrome coronavirus 2 (SARS-CoV-2) emerged in late 2021 and quickly became dominant, in part because of a large number of mutations that allowed escape from existing antibodies. New infection waves have come from other Omicron sublineages. Park *et al*. found that either a vaccination booster or a breakthrough infection elicits neutralization activity against the Omicron variants, but only a breakthrough infection induces an antibody response in the nasal mucosa, which might give better protection against transmission. Testing a panel of antibodies, the authors showed that the antibody S2X324 potently neutralizes all SARS-CoV-2 variants tested, making it a candidate for therapeutic development. A cryo–electron microscopy structure shows how this antibody accommodates Omicron-specific mutations to block binding of the viral spike protein to the human ACE2 receptor across the variants. —VV

Science (ISSN) is published by the American Association for the Advancement of Science. 1200 New York Avenue NW, Washington, DC 20005. The title *Science* is a registered trademark of AAAS.